

The effect of pulsed frequency on the plasma jet force with ultra high-frequency pulsed arc welding

Mingxuan Yang¹ · Zhou Yang¹ · Bojin Qi¹

Received: 17 August 2014 / Accepted: 21 July 2015 / Published online: 8 August 2015
© International Institute of Welding 2015

Abstract Plasma jet force is considered to be the key component of the arc force during arc welding. This is known to be the important factor for surface penetration into the molten pool. With pulsed welding technology, the arc plasma constricts significantly which affects the plasma jet force. The experimental results in this work indicate that the arc force increases with increasing pulse frequency. The plasma jet force is found to be the most important contributor to a larger arc force during ultra high-frequency pulsed gas tungsten arc welding (UHFP-GTAW). In this work, the reason for the increasing force is studied with support from a mathematical model. The plasma jet force was recognized to change with the distribution coefficient a at various pulse frequencies. With increasing frequency, the value of the distribution coefficient decreases. As known, the distribution coefficient represents attenuation of the curve. The results suggest that with a high pulse frequency, a high level of plasma jet force occurs in a constricted arc plasma and significant attenuation of the plasma jet force can be found. In contrast, the plasma jet force was low with little attenuation during conventional gas tungsten arc welding (C-GTAW).

Keywords (IIW Thesaurus) Arc welding · Plasma

Doc. IIW-2574, recommended for publication by Commission XII “Arc Welding Processes and Production Systems”

Zhou Yang contributed equally to the first author of this work.

✉ Mingxuan Yang
yangmingxuan@buaa.edu.cn

¹ Department of Materials Processing, Beijing University of Aeronautics and Astronautics, Beijing 100191, People's Republic of China

1 Introduction

Arc force is a key factor of welding process, which consists of a plasma jet force contribution, an electromagnetic force contribution, an electron force contribution, and so on [1]. The electromagnetic force and plasma jet force are known to be the two most important components of the arc force, while the former is the reason for arc constriction during pulsed welding [2]. The area of arc plasma decreases with high pulsed frequency while the energy density, current density, and heat input increase [3]. Plasma jet force generates an obvious impact force, giving rise not only to convections in molten pool [4–6] but also to the surface depression that can cause more penetration [7, 8]. The radial component of molten convective flow due to the impact force pushes the liquid metal from the center to the edge of the molten pool, which has been described as a plasma drag force in studies of fluid flow in weld pool. The literature indicates that the effect of plasma drag force is much less than Marangoni convection with less than 100-A welding current; however, this becomes much more important when welding current is more than 150 A. The axial component of the arc force was measured and several scholars claim that most of the arc force is due to the plasma jet force (gas dynamic) component [9]. Pulsed welding technology has been demonstrated to have huge impact on arc behavior [10]. In previous work reported, the arc force was influenced significantly with pulsed arc welding compared during conventional GTAW (C-GTAW) [11], especially at ultra high pulsed frequencies ($f > 20$ kHz). The results of the authors indicate that the arc force increases with pulsed frequency [12]. Plasma jet force contributed mostly to the larger arc force with ultra high-frequency pulsed gas tungsten arc welding (UHFP-GTAW), and this varies with pulse frequency f . The distribution of plasma jet force and electromagnetic force has been represented by a two-dimensional model. The results showed that both vary with welding current and root radius of the arc. Most

of the research reports indicate arc constriction with pulsed welding [13–15]. The effect of pulsed current on the arc profile is to change the root radius of the arc. Above all, an improved description of the process can be established with the change of arc profile caused by both electromagnetic force and plasma jet force. Secondly, the relationship between the arc root radius and pulse frequency has been discussed with the aid of a mathematical model, which further correlates between the force and pulse frequency.

In the previous work of the authors, the radial electromagnetic force has been referred to when studying the reason for arc constriction. Plasma jet force is considered as the other key component of the arc force during arc welding, which is also an important factor for the surface depression of the molten pool. As a result, this paper focuses on the plasma jet force in the arc plasma with ultra high-frequency pulse GTAW (UHFP-GTAW). The reason for the increasing arc force during pulsed welding is discussed based on experimental results. Furthermore, a mathematical model of the plasma jet force is established to explore the reason for the increasing arc force with an ultra high pulse frequency. Simultaneously, the distribution of plasma jet force has been analyzed.

2 Methods

2.1 Welding power source

UHFP-GTAW is achieved with an insulated gate bipolar transistor (IGBT) switch component illustrated by Fig. 1, in which

a full- and half-bridge inverter circuit is used. The switch component can withstand voltages of more than 500 V, which secured the high pulsed frequency and large current switching speed di/dt . Compared with previous pulsed welding technology, UHFP-GTAW utilizes pulse frequencies 0–80 kHz and also has up/down current switching rates $di/dt \geq 50$ A/ μ s. The time durations of the background and pulsed currents are t_b and t_p , respectively. The duty cycle δ can be calculated as $t_p/(t_b+t_p)$. The duty cycle determines the ratio of pulsed current during every cycle time. The waveform of the welding current and arc voltage is also illustrated in Fig. 1. An output at 20 kHz pulse frequency was captured (the cycle period is 50 μ s), where 1 is welding current and 2 is the arc voltage. The welding current at 60 kHz is shown in Fig. 2, in which the period cycle is 16.7 μ s.

2.2 Welding experiments and measurements

The pulsed welding parameters are listed in Table 1. With a conventional GTAW process, the welding current was a constant 55 A. By contrast, background and pulsed currents were 30 and 70 A with UHFP-GTAW, respectively. The electrode consisted of a 2.4-mm-diameter tungsten with about 60° electrode included angle. The nozzle diameter was 16 mm. The distance between the electrode and the workpiece was 3 mm (constant, length of arc plasma), and the shielding gas was argon (99.99 %) with volume flow $q_c=12$ L/min. The scale of the workpiece is 100 mm \times 40 mm \times 1.5 mm.

The arc force was measured with the apparatus that is illustrated in Fig. 3a. The measurements were carried out during

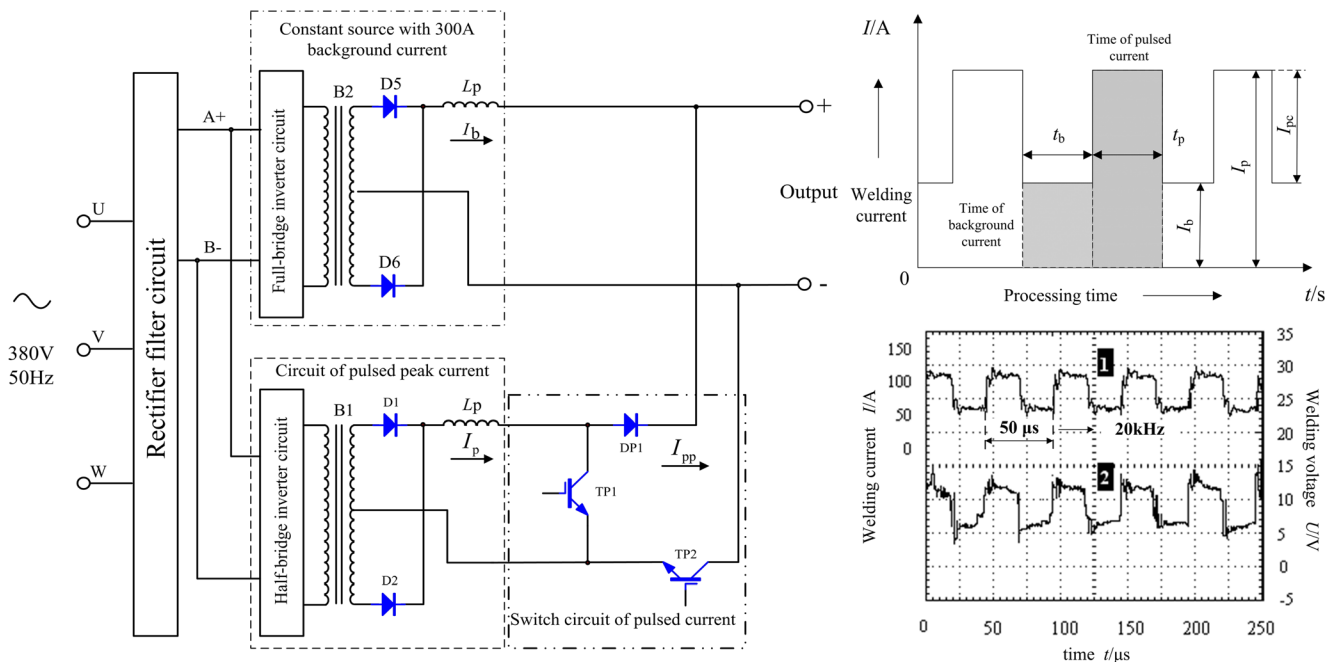


Fig. 1 Schematic and welding output of UHFP-GTAW. I_b background current, I_p pulsed current, I_{pc} amplitude current, I welding current, 2 arc voltage with output capture (20 kHz)

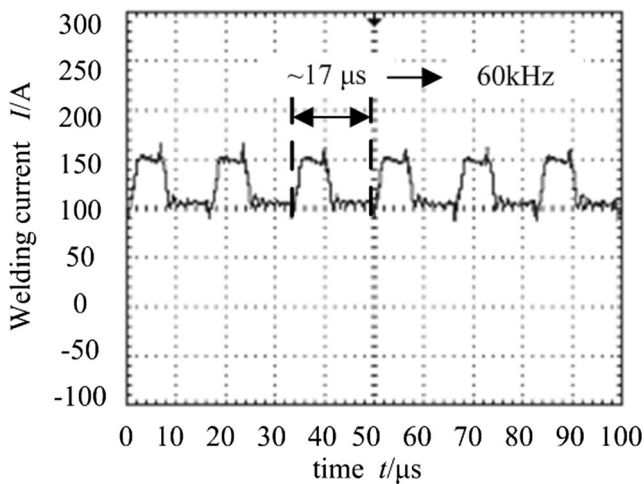


Fig. 2 Welding current with 60 kHz

the process of spot welding, and the process was stable. The measurement results from the sensor were captured on a PC simultaneously with welding process data, during which amplifying and filtering tools were used. The capture frequency was 3 Hz, and the results are the average force. The measured data is displayed in Fig. 3b. Period I was the static period

Table 1 Pulsed welding parameters

No.	Pulsed frequency f/kHz	Background current I_b/A	Pulsed current I_p/A	Duty cycle $\delta/\%$
1	–	55		
2	10	30	70	50
3	20	30	70	50
4	25	30	70	50
5	30	30	70	50
6	35	30	70	50
7	40	30	70	50
8	42	30	70	50
9	45	30	70	50
10	48	30	70	50
11	50	30	70	50
12	52	30	70	50
13	55	30	70	50
14	58	30	70	50
15	60	30	70	50
16	62	30	70	50
17	65	30	70	50
18	68	30	70	50
19	70	30	70	50
20	72	30	70	50
21	75	30	70	50
22	78	30	70	50
23	80	30	70	50

before welding. The arc was ignited at the welding start time. Period II is the measured period with a stable welding arc; this continued until welding ended. Finally, period III is the static period after welding. The average drop of measured data between periods I and II is recognized as the arc force. The reduction in force in period II is due to metal vapor loss during welding.

2.3 Model for plasma jet force

As mentioned before, electromagnetic force and plasma jet force are the main components of the arc force. Previous work [16] discussed the electromagnetic force with UHFP-GTAW, and the results indicated that it decreased with arc constriction. However, the pressure caused by electromagnetic force has not yet been taken into account. The measured results suggested a high arc force which can be found at high pulsed frequency as will be described in Section 3. Thus, the plasma jet force is predicted to be the most important factor for the increasing arc force.

Various mathematical models were chosen for the analysis of the welding process. As known, Gaussian and double-sided exponential distributions are usually used to describe the plasma jet force in the arc plasma. Gaussian has proven to be applicable to plasma welding [17] and a double-sided exponential distribution to GTAW. First of all, the root of the arc is assumed to be circle during arc spot welding. The distribution on the arc root can be simplified to a line distribution on the surface illustrated in Fig. 4. The line function P_r can be written as Eq. 1, shown below, which is used to describe the plasma pressure distribution. The average line distribution function of plasma pressure $\overline{P_{r\text{-line}}}$ is integrated from Eq. 2 using Eq. 1. In the arc root, the line distribution of plasma pressure was integrated over the angle θ in Eq. 3. Next, Eq. 1 is modified to Eq. 4 to represent arc force, in which peak pressure is assumed to be $F_{\text{max}}/\pi R_r^2$ in this section. Combining Eqs. 1~4, we obtain function for the average plasma jet force at the arc root as shown in Eq. 5. During subsequent analysis, the calculations were carried out with Eq. 5 which is recognized as the relative value of the plasma jet force. Notice that the unit of the distribution coefficient is m^{-1} .

$$P_r = P_{\text{peak}} \exp(-a|r|) \tag{1}$$

where P_r is the plasma pressure of the arc, P_{peak} is the pressure on the axial, a is the distribution coefficient (m^{-1}), and r is the radial coordinate.

$$\overline{P_{r\text{-line}}} = \frac{\int P_r dr}{2r} \tag{2}$$

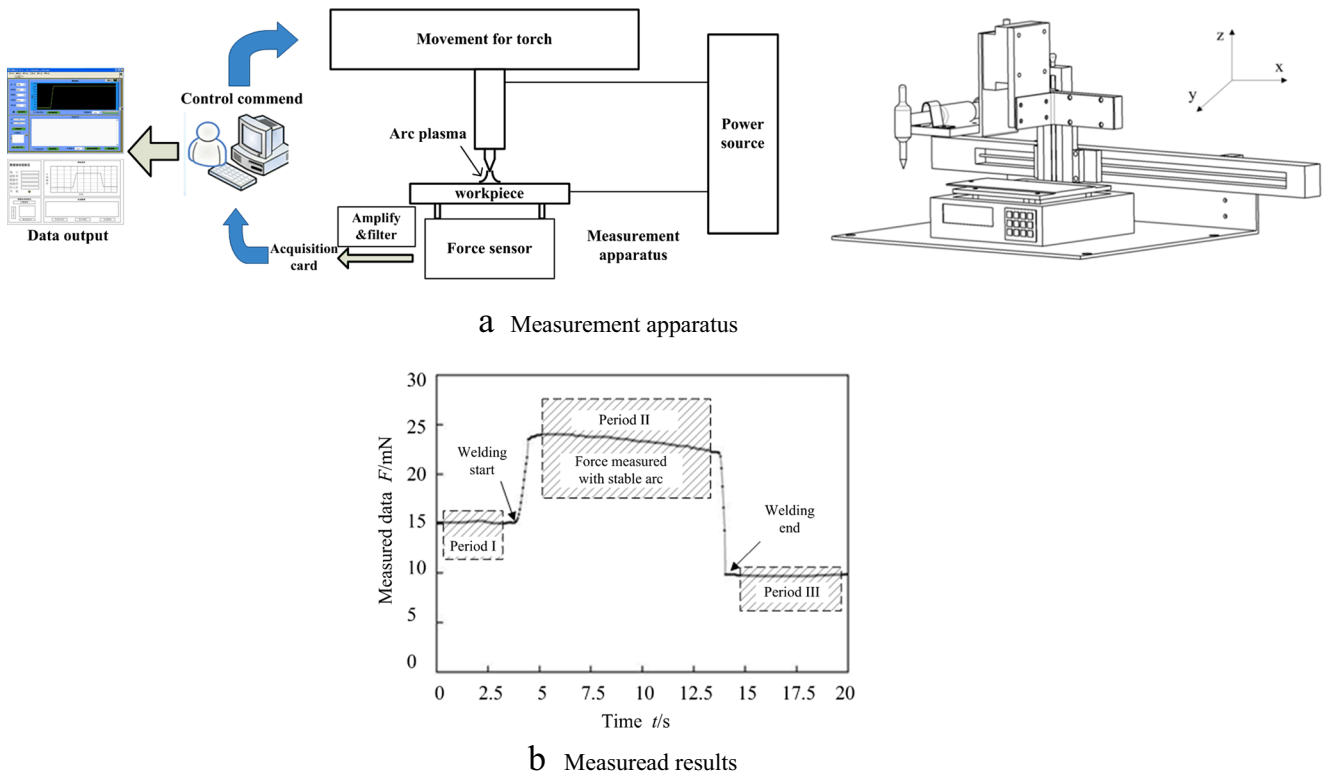


Fig. 3 Apparatus for arc force measurement. **a** Measurement apparatus. **b** Measured results

where $\overline{P_{r-line}}$ is the line distribution function of plasma pressure and P_r is the plasma pressure at the radial coordinate r in the arc root.

$$\overline{P_r} = \int \overline{P_{r-line}} d\theta \tag{3}$$

where $\overline{P_r}$ is the distribution function of plasma pressure in arc root integrated over the circle described by the angle θ

$$P_r = P_{peak} \exp(-a|r|) = \frac{F_{max}}{\pi R_r^2} \frac{a^2 r^2}{2[1 - e^{-ar}(1 + ar)]} \tag{4}$$

where F_{max} is the force on the axial.

$$\begin{aligned} \overline{F_r} &= \int_0^\pi \int_{-R_r}^{R_r} \frac{1}{2r} F_r dr d\theta = \int_0^\pi \int_{-R_r}^{R_r} \frac{1}{2r} P_r \cdot \pi \cdot r^2 dr d\theta \tag{5} \\ &= \frac{\pi a^2 F_{max}}{2R_r^2} \int_0^{R_r} \frac{r^3}{1 - e^{-ar}(1 + ar)} e^{-ar} dr \end{aligned}$$

3 Results and discussion

3.1 The arc force experimental results

The experimental results indicate that the arc force with UHFP-GTAW process is much greater than with C-GTAW. Figure 5 illustrates the trend of the arc force varying with pulse frequency, from which the arc force has been represented with functions of the pulsed frequency by Eqs. 6–8 below. The

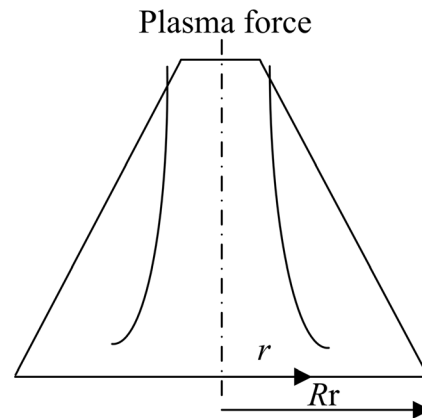
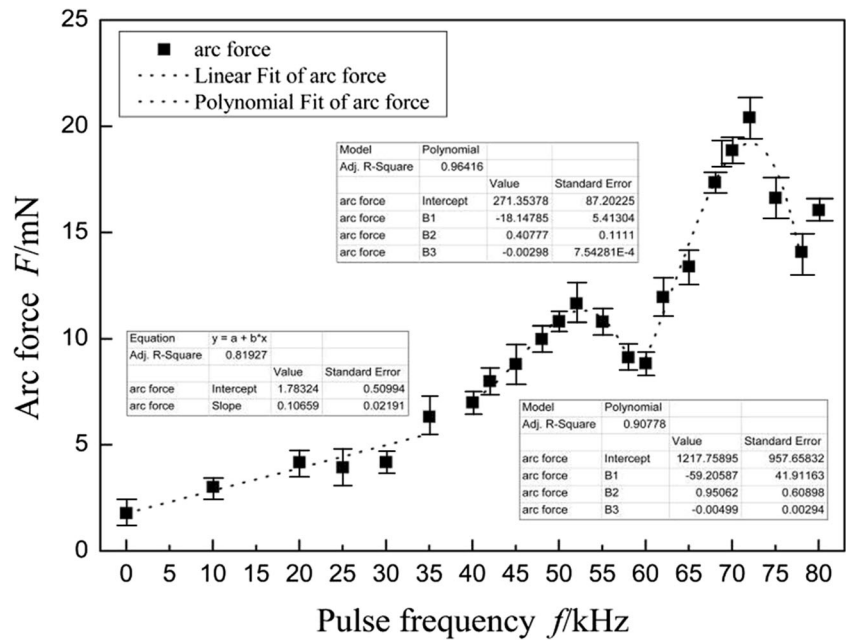


Fig. 4 2-D model of plasma jet force. r the radial coordinate of the arc root, R_r is the radius of the arc root

Fig. 5 Experimental results for the measured arc force



initial point of pulse frequency is the arc force with C-GTAW in this figure. For each pulsed frequency, the measured result is averaged with at least three sets of valid data. The measured arc force shows a significant increment with UHFP-GTAW, and the maximum force measured reached up to almost 800 % of the C-GTAW measured force.

$$\text{When } f \in [0, 40)_{\text{kHz}} \quad \phi(f) = 0.11 \cdot f + 1.78, \quad R^2 = 0.8193 \quad (6)$$

$$\text{When } f \in [40, 60)_{\text{kHz}} \quad \phi(f) = -0.003 \cdot f^3 + 0.41 \cdot f^2 - 18.15 \cdot f + 271.35, \quad R^2 = 0.9642 \quad (7)$$

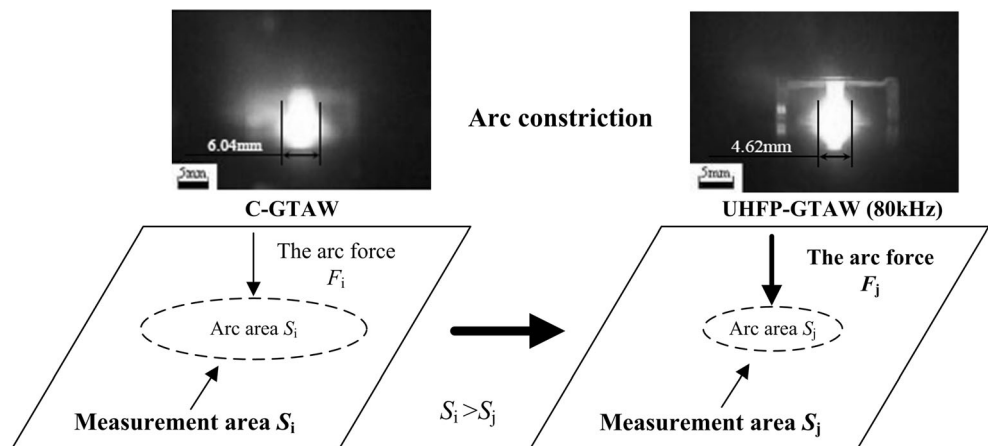
$$\text{When } f \in [60, 80)_{\text{kHz}} \quad \phi(f) = -0.005 \cdot f^3 + 0.95 \cdot f^2 - 59.21 \cdot f + 1217.76, \quad R^2 = 0.9078 \quad (8)$$

The *R*-square value suggests that the arc force can vary with pulse frequency following a polynomial form. With different pulsed frequencies, various types of curves were

observed. Notice that the linear fitting was used when pulsed at less than 40 kHz (pulse frequency). With 40~80 kHz (pulsed frequency), third-order polynomial fitting was carried out to describe the correlation between the arc force and the pulsed frequency. The results demonstrated the third-order polynomial is considered to be suitable for the arc force with UHFP-GTAW. Above all, we inferred that a mathematical correlation may exist between the arc force and pulsed frequency over the range of frequencies examined in the experiments. As described in Section 2, the plasma jet force is the key factor contributing to the high arc force during pulsed arc welding, and the reason will be analyzed below.

The discussion above presented the correlation between arc force and pulsed frequency. Such correlation is shown in this work supported by both experiments and mathematical analysis. It is also evidence for a direct relationship between arc behavior factors and

Fig. 6 Arc force measurement with arc constriction



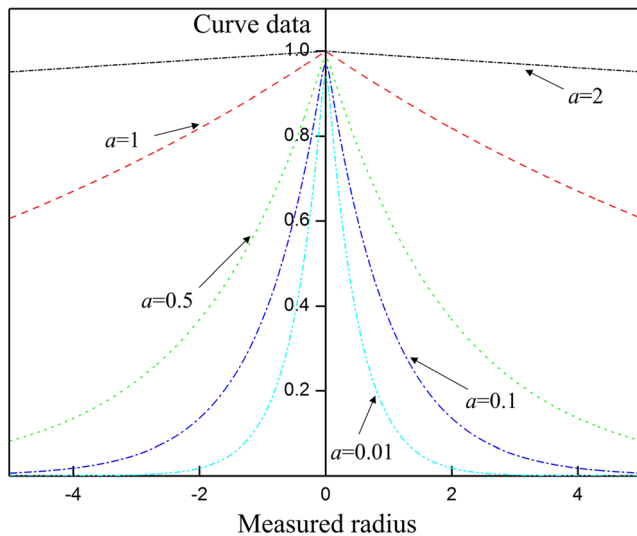


Fig. 7 Correlation curves with distribution coefficient

pulsed frequency parameters. These results will be important for further study on arc behavior with pulsed welding processes. Additionally, the scale of the workpiece, especially the thickness, is supposed to influence the measured results partly as the forced vibration may occur in thin plate. Measurements with thick plate (more than 5 mm) will be carried out in further study to evaluate the prediction.

3.2 The electromagnetic force

In ref [16], the pressure of the axial electromagnetic force increased (by about 30 % at most) with the arc constriction, although the absolute value of the force decreased (by 25 %). The results indicate that the axial electromagnetic force is the factor that will create liquid surface deformation. Our previous description focused on the effect of electromagnetic force, which can be discussed with respect to pressure and arc constriction. Figure 6 illustrates the arc force measuring process with arc constriction.

The arc force $F_{(measured)}$ can be written to be a function of pressure as $P=F_{(measured)}/S_n$. With Fig. 6, the force without/with arc constriction can be found during C-GTAW and UHFP-GTAW respectively. The results produced that $F_{i(\text{the arc force without constriction})} < F_{j(\text{the arc force with constriction})}$ and the area $S_i > S_j$. According to the pressure function above, larger pressure can be deduced with F_j , a surface depression with an axial electromagnetic force. However, the measured arc force

increased by 150~800 % with the experiments that meant such significant increasing force may be due to other factors.

3.3 The plasma jet force

As described before, the electromagnetic force and plasma jet force are the main contributions to the arc force. The former shows a decreasing value with arc constriction. However, the pressure increased because of the small area with UHFP-GTAW. That meant the effect of the axial electromagnetic force cannot be ignored when studying surface depression of the molten pool. Conversely, the measured results indicated a high arc force with pulsed arc welding.

The distribution coefficient a can be used to represent the fluctuation of the functions as mentioned before. From Eq. 5, the average plasma jet force can be represented in terms of root radius and distribution coefficient. The former has been calculated based on photographs captured by a camera system. Various root radii can be listed with different pulsed frequencies with both experimental results and calculation. And notice that the discussion is under one certain distribution coefficient a . Similarly to the calculation during heat input model analysis, the distribution coefficient is $3/r^2$, which determines the curvature of the correlation curve (Fig. 7). Here, r is the measured radius. A large distribution coefficient corresponds to significant attenuation of the function output.

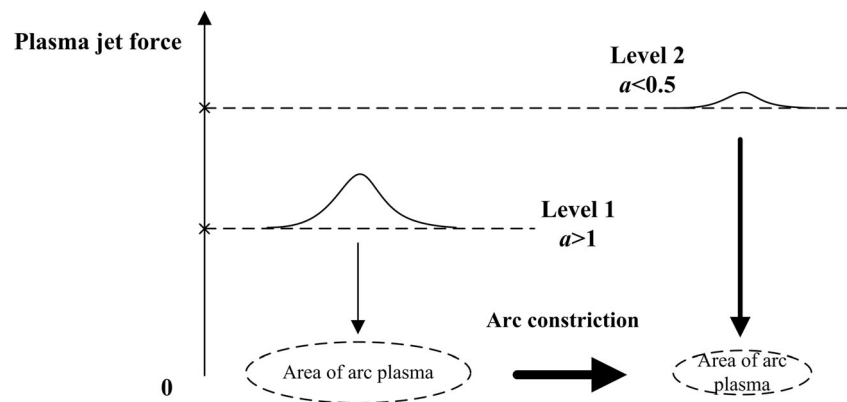
A verifying test was carried out with certain distribution coefficient. With a certain distribution coefficient value (ex. $a=1.2$), the calculated results with different pulsed frequencies are illustrated in Table 2. It is found that the increase rates are between 7 and 26 % with different frequencies, which are much less than 150~800 % that was measured in the experiment. Such results can also be achieved with other distribution coefficients. As described above, the pressure can increase by about 300 % at most which is also far from the experimental results.

In addition, the calculated results will be similar to the trend of arc force F - f according to the traditional physical view that was mentioned in Section 1. However, the change of value was less than 30 % at all of the frequencies in Table 2. The experimental results indicate that the calculated value cannot be matched with any certain distribution coefficient a . The graph suggests that there is no obvious increment with any coefficient, and no curve can match the trend of the arc force observed in the experiments. Furthermore, we infer that the results above may demonstrate that the distribution coefficient

Table 2 Approaching results of plasma jet force distribution

Pulsed frequency f /kHz	0	20	25	30	35	40	45
Approaching value	0.3623	0.3883	0.3869	0.3921	0.4038	0.3933	0.4091
Pulsed frequency f /kHz	50	55	60	65	70	75	80
Approaching value	0.4213	0.418	0.4124	0.4158	0.4431	0.4374	0.4571

Fig. 8 Schematic of plasma jet force with different distribution coefficient



changes with different pulse frequencies. The distribution coefficient decreases while high pulse frequencies increase. The coefficient changed from more than one to less than 0.5 with different pulsed frequencies. As described before, the distribution coefficient represents the fluctuation of original functions. As a result, with low value of the distribution coefficient, the fluctuation of the curve will reduce which causes the plasma jet force to be stabilized at high pulse frequencies. The reason for such phenomenon is described below.

During UHFP-GTAW, significant arc constriction can be found with the experimental results from Section 1. The distribution region of the arc force decreases. Actually, the average plasma jet force in Section 2 can be described as the distribution itself. Thus, with high pulsed frequency, the large level of plasma jet force distributes in the constricted arc plasma and less attenuation exists. By contrast, the force was at a low level with C-GTAW or low pulsed frequency as illustrated in Fig. 8. With increasing pulsed frequency, the area of the arc plasma reduced with a high level of the force at level 2 in Fig. 8. The average force reached a high level, and little attenuation was observed. Compared with this, a conventional attenuation function can be found for C-GTAW or low pulse frequencies as level 1 (in Fig. 8).

4 Conclusion

- (1) The experimental results indicate that the arc force increases with higher pulsed frequency (150–800 %). The plasma jet force is found to be the most significant contributor to a larger arc force in UHFP-GTAW.
- (2) With the change of pulsed frequency, the increasing rates of both electromagnetic force and plasma jet force cannot explain the observed experimental results of the arc force. However, the pressure caused by them reaches 300 % at most, which was due to a significant arc constriction.
- (3) The plasma jet force distribution coefficient may change during UHFP-GTAW. The coefficient tends to be smaller

with increased pulsed frequency. The results infer that the fluctuation of plasma jet force decreases with UHFP-GTAW. The force was stabilized at a higher level at high pulsed frequency.

Acknowledgments This work was supported by the National Natural Science Foundation of China under grant No. 51405007 and Fundamental Research Funds for Central Universities. The authors acknowledge Beijing University of Aeronautics and Astronautics for supporting the research work.

References

1. Ando K, Hasegawa M (1985) Welding arc phenomena. Beijing, pp 249–250
2. Cook GE, Eassa EDEH (1985) The effect of high-frequency pulsing of a welding arc. *IEEE Trans Ind Appl IA-21(5)*:1294–1299
3. Murphy AB, Tanaka M, Yamamoto K et al (2009) Modelling of thermal plasmas for arc welding: the role of the shielding gas properties and of metal vapour. *J Phys D Appl Phys* 42(19):194006
4. Choo RTC, Szekely J (1991) The effect of gas shear stress on Marangoni flows in arc welding. *Weld J* 70(9):223–233
5. Ko SH, Yoo CD, Choi SK (2001) Effects of surface depression on pool convection and geometry in stationary GTAW. *Weld J* 80(2): 39–45
6. Kim WH, Fan HG, Na SJ (1997) Effects of various driving forces on heat and mass transfer in arc welding. *Numer Heat Transfer, Part A* 32(6):633–652
7. Oreper GM, Szekely J (1987) A comprehensive representation of transient weld pool development in spot welding operations. *Metall Mater Trans A* 18(7):1325–1332
8. Qi BJ, Yang MX, Cong BQ et al (2013) The effect of arc behavior on weld geometry by high frequency pulse GTAW process with 0Cr18Ni9Ti stainless steel. *Int J Adv Manuf Technol* 66(12): 1545–1553
9. Jia CS, Xiao KM, Yin XQ (1994) Plasmas flow force of welding arc. *Trans China Weld Inst* 15(2):101–106
10. Ghosh PK, Dorn L, Hübner M et al (2007) Arc characteristics and behavior of metal transfer in pulsed current GMA welding of aluminum alloy. *J Mater Process Technol* 194:163–175
11. Onuki J, Anazawa Y, Nihei M et al (2002) Development of a new high-frequency, high-peak current power source for high constricted arc formation. *J Appl Phys* 41:5821–5826

12. Qi BJ, Yang MX, Cong BQ et al (2012) Study on fast-convert ultrasonic frequency pulse TIG welding arc characteristic. *Mater Sci Forum* 704–705:745–751
13. Amin M (1983) Pulse current parameters for arc stability and controlled metal transfer in arc welding. *Met Constr* 15:272–278
14. Tušek J (2000) Experimental investigation of gas tungsten arc welding and comparison with theoretical predictions. *IEEE Trans Plasma Sci* 28(5):1688–1693
15. Greenfield S, Jones I, Berry CT (1964) High-pressure plasma as spectroscopic emission source. *Analyst* 89:713–720
16. Yang MX, Qi BJ, Cong BQ et al (2013) Study on electromagnetic force in arc plasma with UHFP-GTAW of Ti-6Al-4V. *IEEE Trans Plasma Sci* 41(9):2561–2568
17. Fan HG, Kovacevic R (1999) Keyhole formation and collapse in plasma arc welding. *J Phys D Appl Phys* 32(22):2902–2909